Endogenous agonist–bound S1PR3 structure reveals determinants of G protein–subtype bias

AUTHOR(S):

Maeda, Shintaro; Shiimura, Yuki; Asada, Hidetsugu; Hirata, Kunio; Luo, Fangjia; Nango, Eriko; Tanaka, Nobuo; ... Aoki, Junken; Iwata, So; Hagiwara, Masatoshi

CITATION:

Maeda, Shintaro ...[et al]. Endogenous agonist–bound S1PR3 structure reveals determinants of G protein–subtype bias. Science Advances 2021, 7(24): eabf5325.

ISSUE DATE:

2021-06

URL:

http://hdl.handle.net/2433/263316

SCIENCE ADVANCES | RESEARCH ARTICLE

STRUCTURAL BIOLOGY

Endogenous agonist–bound S1PR3 structure reveals determinants of G protein–subtype bias

Shintaro Maeda[1,2], Yuki Shiimura[3,4], Hidetsugu Asada[3], Kunio Hirata[5], Fangjia Luo[3,5], Eriko Nango[3,5,6], Nobuo Tanaka[7], Masayasu Toyomoto[1,8], Asuka Inoue[9], Junken Aoki[9†], So Iwata[3,5]*, Masatoshi Hagiwara[1,2,7,8]*

Sphingosine-1-phosphate (S1P) regulates numerous important physiological functions, including immune response and vascular integrity, via its cognate receptors (S1PR1 to S1PR5); however, it remains unclear how S1P activates S1PRs upon binding. Here, we determined the crystal structure of the active human S1PR3 in complex with its natural agonist S1P at 3.2-Å resolution. S1P exhibits an unbent conformation in the long tunnel, which penetrates through the receptor obliquely. Compared with the inactive S1PR1 structure, four residues surrounding the alkyl tail of S1P (the "quartet core") exhibit orchestrating rotamer changes that accommodate the moiety, thereby inducing an active conformation. In addition, we reveal that the quartet core determines G protein selectivity of S1PR3. These results offer insight into the structural basis of activation and biased signaling in G protein–coupled receptors and will help the design of biased ligands for optimized therapeutics.

INTRODUCTION

G protein–coupled receptors (GPCRs) form the largest superfamily of transmembrane proteins that transduce signals to the interior of cells in response to extracellular stimuli (*1*). The binding of GPCR agonists activates heterotrimeric G protein–mediated downstream signaling dependent on each subunit (Gα, Gβ, and Gγ) (*2*–*4*). In humans, Gα subunits are encoded by 16 genes and classified into four major families (G_s, $G_{i/o}$, $G_{q/11}$, and $G_{12/13}$) that trigger distinct signaling cascades. Although many GPCRs couple with multiple Gα families upon activation, the activated Gα-mediated signaling pathways are ligand dependent in a process referred to as "biased agonism" (*5*, *6*). Although unbiased agonism transduces several intrinsic signaling pathways via its own receptor, biased agonists selectively transduce specific signaling pathways and can enhance therapeutic efficacy or diminish side effects (*7*). For example, endogenous agonists that activate $G_{i/o}$ rather than $G_{q/11}$ subunits via chemokine receptor 5 potentially block HIV-1 infection without inducing inflammation (*8*). Despite recent advances in our understanding of GPCR–G protein coupling (*9*–*13*), it remains elusive how ligands in the ligand-binding pocket change the intracellular conformation of receptors to modulate signaling-pathway selectivity.

Sphingosine-1-phosphate (S1P) is a lysophospholipid characterized by a single alkyl chain and was initially identified as a phospholipid precursor and metabolite (*14*). S1P is a signaling molecule that acts through five GPCRs (S1PR1 to S1PR5) (*15*–*17*), among which S1PR3 couples to $G_{q/11}$, $G_{i/o}$, and $G_{12/13}$ upon S1P binding and regulates immune responses including P-selectin–dependent leukocyte rolling via a $G_{q/11}$-mediated signaling (*18*), cellular chemotaxis stimulation via a $G_{i/o}$-mediated signaling, and cellular chemotaxis inhibition via a $G_{12/13}$-mediated signaling (*19*, *20*). A previous study of S1PR3 showed that phosphorylated fingolimod (FTY720-P), a structural analog of S1P characterized by a shorter lipidic tail containing a phenyl acyl group, exerted $G_{i/o}$-biased agonism of S1PR3 (*21*). The underlying mechanism on how the alkyl tail length of ligands determines the G protein selectivity of S1PR3 was, however, unclear.

Structural examination of S1PR1 in complex with the sphingosine-mimic antagonist ML056 (*22*) provides molecular basis of the inactive state of the S1PRs yet does not inform us as to how S1PRs are activated. To gain insight into the S1PR-activation mechanism, here, we report the crystal structure of human S1PR3 in complex with its natural agonist d18:1 S1P. The results show that the ligand-binding pocket forms a long penetrating tunnel not seen in other GPCRs. Furthermore, the structure reveals that amino acid residues involved in formation of the long tunnel play an important role in the receptor activation and biased agonism.

RESULTS

Determination of the S1PR3 structure

To prepare protein for crystallization, we designed a construct encoding human S1PR3 (hS1PR3) lacking the C terminus (residue range: 316 to 378) and introduced an Asn15Gln mutation to remove the *N*-glycosylation site. Purified hS1PR3 was incubated with d18:1 S1P and a Fab antibody fragment specific for hS1PR3 (Fab AS55). Following size exclusion chromatography (SEC), the complex was crystallized using the lipidic cubic phase (LCP) method (fig. S1A), resulting in needle-like crystals obtained within 1 week (fig. S1, B and C) and allowing determination of the S1PR3 structure at 3.2-Å resolution (table S1). The crystals contain two d18:1 S1P–S1PR3–Fab AS55 complexes in the crystallographic asymmetric unit (fig. S1, D

[1]Department of Anatomy and Developmental Biology, Graduate School of Medicine, Kyoto University, Kyoto 606-8501, Japan. [2]Department of Drug Discovery Medicine, Graduate School of Medicine, Kyoto University, Sakyo-ku, Kyoto 606-8507, Japan. [3]Department of Cell Biology, Graduate School of Medicine, Kyoto University, Sakyo-ku, Kyoto 606-8501, Japan. [4]Institute of Life Science, Kurume University, Kurume, Fukuoka 830-0011, Japan. [5]RIKEN SPring-8 Center, Sayo-cho, Sayo-gun, Hyogo 679-5165, Japan. [6]Institute of Multidisciplinary Research for Advanced Materials, Tohoku University, 2-1-1 Katahira, Aoba-ku, Sendai 980-8577, Japan. [7]Medical Research Support Center, Graduate School of Medicine, Kyoto University, Sakyo-ku, Kyoto 606-8501, Japan. [8]Department of Drug Discovery for Lung Diseases, Graduate School of Medicine, Kyoto University, Kyoto 606-8501, Japan. [9]Laboratory of Molecular and Cellular Biochemistry, Graduate School of Pharmaceutical Sciences, Tohoku University, Sendai, Miyagi 980-8578, Japan.
*Corresponding author. Email: hagiwara.masatoshi.8c@kyoto-u.ac.jp (M.H.); (s.iwata@mfour.med.kyoto-u.ac.jp (S.I.)
†Present address: Department of Health Chemistry, Graduate School of Pharmaceutical Sciences, The University of Tokyo, 7-3-1 Bunkyo-ku, Hongo, Tokyo 113-0033, Japan.

to I). Fab AS55 recognizes extracellular domains of S1PR3 including N-terminal loop (fig. S2).

The overall structure of S1PR3 shows the canonical seven-transmembrane bundles holding the unbent d18:1 S1P (Fig. 1A). This structure shares common features with a previously determined inactive S1PR1 structure in complex with the sphingosine-mimic antagonist (*22*), including the extracellular lid composed of the N-terminal helix, extracellular loop 2 (ECL2), and ECL3 (Fig. 1, B and C). The N-terminal region forms a helical cap and contributes to ligand interaction, and disulfide bonds are formed in ECL2 (Cys178-Cys185) and ECL3 (Cys269-Cys274). These extracellular structures block ligand access from the extracellular region and are conserved in both reported S1P receptors. These findings strongly suggest that ligand entry to the binding pocket of S1PRs occurs primarily from the membrane bilayer through the side gap between helical transmembrane domain 1 (TM1) and TM7 (Fig. 1, B and C).

A notable difference between the d18:1 S1P–bound S1PR3 structure and the antagonist-bound S1PR1 structure is observed in the lower parts of the ligand-binding pockets. Active S1PR3 has a long tunnel structure crossing from the nearby extracellular end of TM1-TM2-TM7 through the gap between TM4 and TM5 and accommodates unbent d18:1 S1P, whereas inactive S1PR1 has bifurcated shallow hydrophobic pockets (Fig. 1, B to E). This difference may be attributed to S1PR activation and has not been identified in previously determined structures of agonist-bound lipid GPCRs (Fig. 1, F to H) (*12*, *23*–*25*).

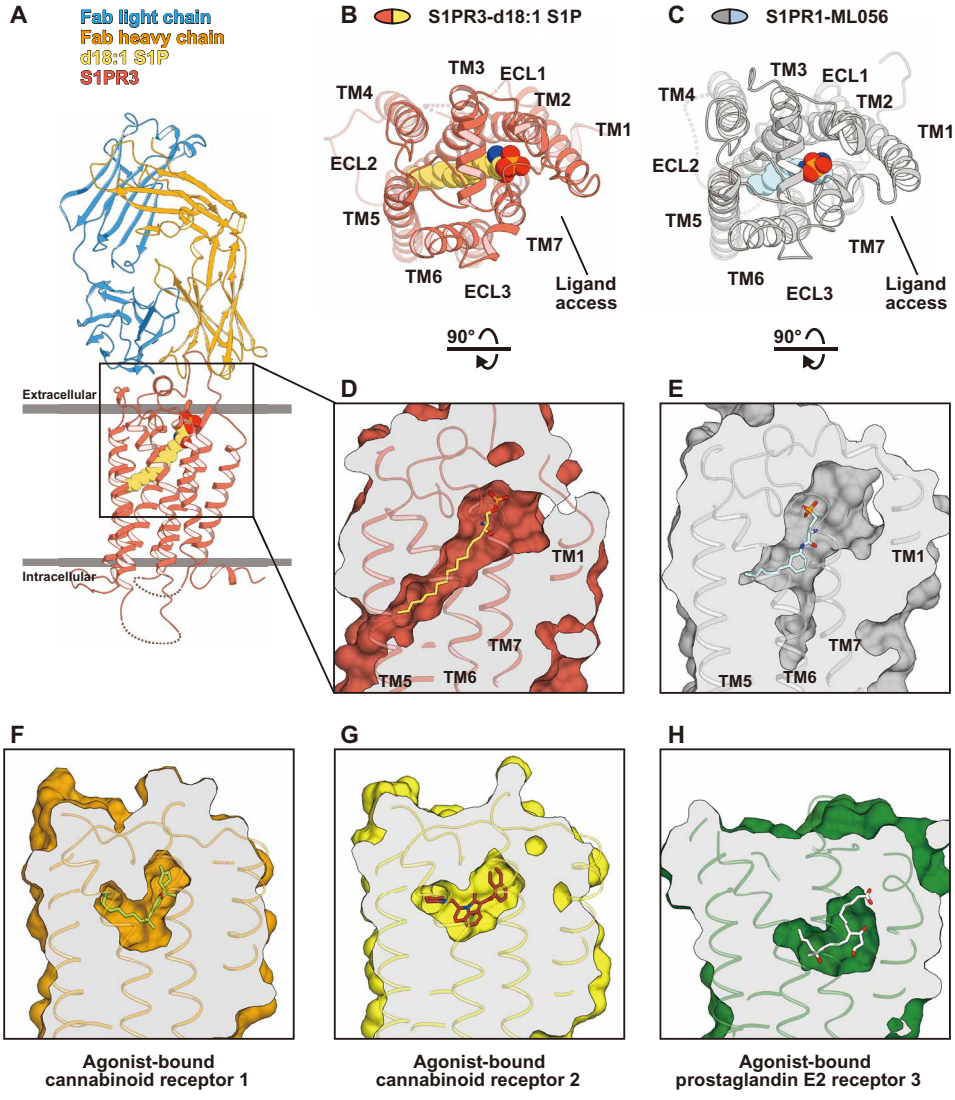

Fig. 1. Overall structure of d18:1 S1P–bound S1PR3. (**A**) Overall structure of the d18:1 S1P–S1PR3–Fab AS55 complex. d18:1 S1P is shown as a space-filling model, with carbon atoms in yellow, nitrogen in blue, oxygen in red, and phosphorus in orange. S1PR3 is colored dark salmon. Fab light chain is colored blue, and Fab heavy chain is colored orange. (**B** and **C**) Extracellular view of the d18:1 S1P–bound S1PR3 structure (B) (PDB ID: 7C4S) and antagonist (ML056)–bound S1PR1 structure (C) (PDB ID: 3V2Y). Each molecule is colored as follows: S1PR3, dark salmon; d18:1 S1P, yellow; S1PR1, dark gray; and ML056, light blue. TM, helical transmembrane domain; ECL, extracellular loop. (**D** to **H**) Cross section of the following structures: (D) d18:1 S1P–bound S1PR3, (E) antagonist (ML056)–bound S1PR1 structure (*22*), (F) AM11542 (agonist)–bound CNR1 (*23*), (G) WIN 55,212-2 (agonist)–bound CNR2 (*12*), and (H) misoprostol (agonist)–bound PTGER3 (*25*).

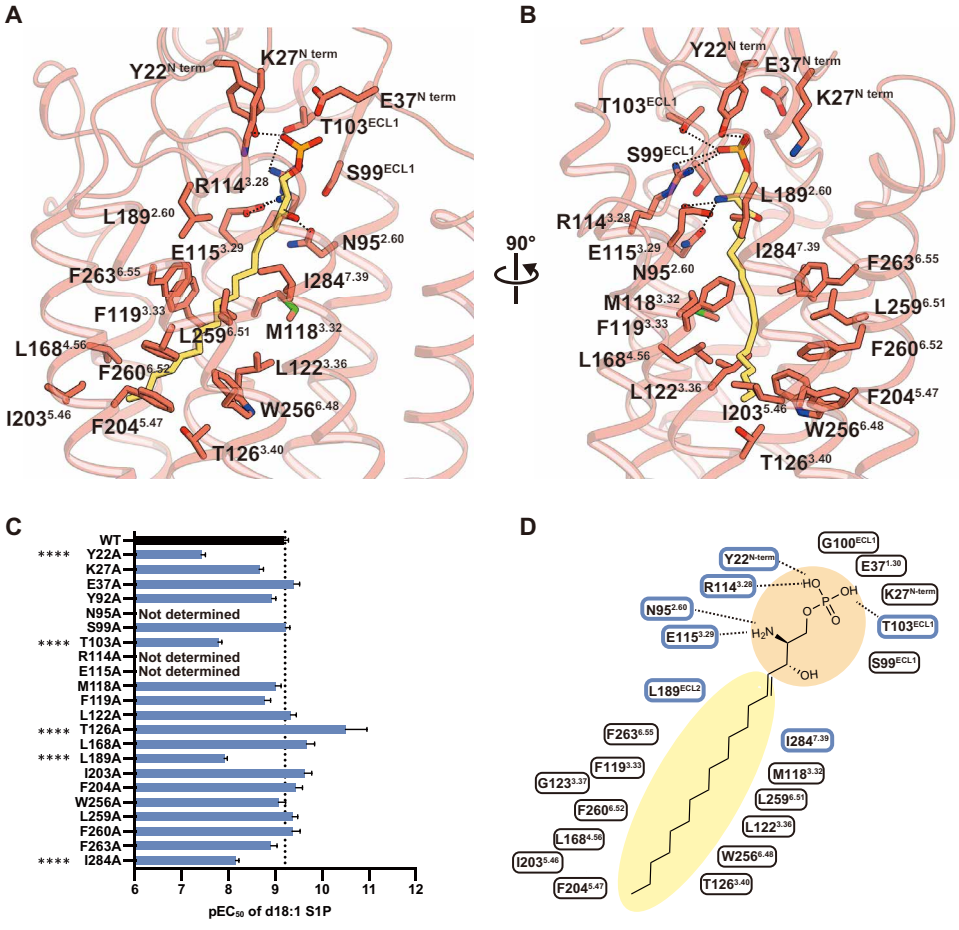

Fig. 2. d18:1 S1P binding mode. (**A** and **B**) Views of residues interacting with d18:1 S1P in the d18:1 S1P–S1PR3–Fab AS55 complex (A) with views rotated 90° counterclockwise (B). The ligand-binding residues in S1PR3 are shown as a licorice model in dark salmon. Hydrogen bonds are shown as black dashed lines. (**C**) Comparison of pEC_{50} values of d18:1 S1P in TGFα shedding assay with HEK293 parental cells expressing mutant and wild-type S1PR3. pEC_{50} values of mutant S1PR3 N95A, R114A, and E115A were estimated to be very low according to the dose-response curve in fig. S4. ****$P < 0.0001$, mutant versus wild-type pEC_{50} values according to one-way analysis of variance (ANOVA) and Dunnett's post test. (**D**) Schematic of the interaction between d18:1 S1P and S1PR3. Hydrogen bonds and salt bridges are shown as black dashed lines. Critical residues for d18:1 S1P binding according to mutation analyses are shown in blue boxes.

S1P-binding mode

The ligand-binding pocket of S1PR3 is highly amphipathic, which is ideal for a hydrophobic-zwitterionic ligand such as S1P (Fig. 2, A and B). The phosphate moiety and amine moiety of d18:1 S1P are surrounded by polar residues, whereas the alkyl tail is surrounded by hydrophobic residues (Fig. 2, A and B). The phosphate moiety of d18:1 S1P forms hydrogen bonds with $Tyr22^{N\text{-}term}$ and $Thr103^{ECL1}$ and a salt bridge with $Arg114^{3.28}$ [superscripts refer to Ballesteros-Weinstein numbering (*26*)]. The amine moiety forms hydrogen bonds with $Glu115^{3.29}$ and $Asn95^{2.60}$. To verify the functional roles of these residues experimentally, we performed mutagenesis analyses using the transforming growth factor–α (TGFα) shedding assay, which reflects $G_{q/11}$ and $G_{12/13}$ signaling. Alanine substitutions of $Tyr22^{N\text{-}term}$, $Asn95^{2.60}$, $Thr103^{ECL1}$, $Arg114^{3.28}$, and $Glu115^{3.29}$ reduced d18:1 S1P potency (Fig. 2, C and D; fig. S3, A and B; and table S2). As previously reported, these polar residues are important for high-affinity interaction with zwitterionic S1P with reference to the sphingosine-mimic antagonist–bound S1PR1 structure (*22*). Meanwhile, alanine substitutions of almost all residues around the alkyl tail of d18:1 S1P, except for $Leu189^{ECL2}$ and $Ile284^{7.39}$, had little effect on d18:1 S1P affinity. These data suggest that polar interactions with the amine and phosphate moieties are more important for S1P binding than hydrophobic interaction with the alkyl tail (Fig. 2, C and D; fig. S3, C and D; and table S2).

Ligand length effects on G protein signaling

As mentioned above, the difference between active S1PR3 and inactive S1PR1 is seen in the lower parts of the ligand-binding pocket that accommodate the alkyl tail of ligands, suggesting that the interaction of the ligands' alkyl tail with receptors decides ligand activity (Fig. 1, D and E). We thus hypothesized that the shorter lipidic tail of FTY720-P relative to d18:1 S1P is a determinant for G protein–subtype bias (Fig. 3A). To test this, we profiled each G protein–dependent S1PR3 signaling pathway using d16:1 S1P, which is an S1P analog with two fewer carbons in the alkyl chain than d18:1 S1P. To evaluate G protein coupling, we performed a GloSensor cyclic adenosine monophosphate (cAMP) accumulation assay to detect $G_{i/o}$-dependent cAMP inhibition and a TGFα shedding assay (*27*, *28*) to detect $G_{q/11}$- and $G_{12/13}$-dependent signaling (fig. S4A). The TGFα shedding assay showed $G_{q/11}$- and $G_{12/13}$-dependent a disintegrin and metalloprotease 17 (ADAM17)–induced~ metallopeptidase domain

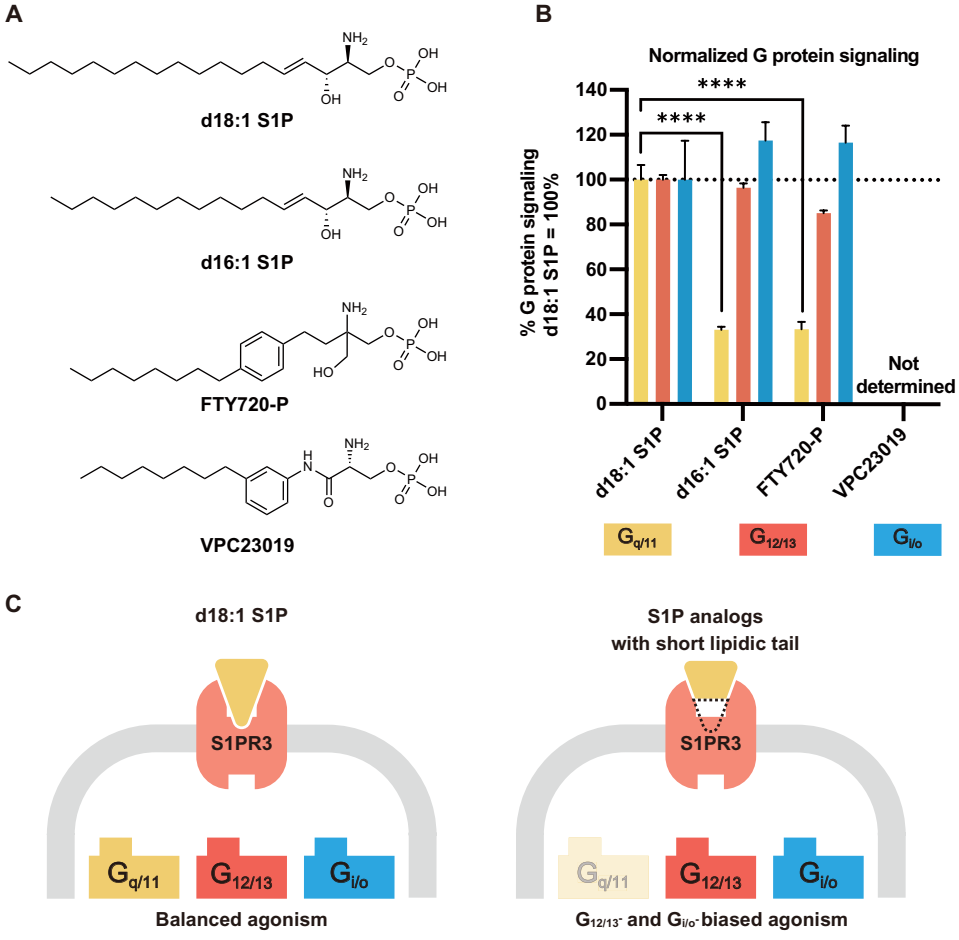

Fig. 3. Short sphingolipids represent $G_{12/13}$- and $G_{i/o}$-biased agonists for S1PR3. (**A**) Chemical structures of ligands used for signaling assays. (**B**) Normalized G protein signaling efficacy. E_{max} of each G protein subtype–specific signaling in response to d18:1 S1P was normalized to 100%. Each bar is colored as follows: $G_{q/11}$, yellow; $G_{12/13}$, salmon; and $G_{i/o}$, light blue. ****$P < 0.0001$, d18:1 S1P versus S1P analogs % G protein signaling according to two-way ANOVA followed by Dunnett's post test. (**C**) Schematic summary of biased agonism in S1PR3. Major S1P, d18:1 S1P, induces $G_{q/11}$-, $G_{12/13}$-, and $G_{i/o}$-dependent signaling via S1PR3. On the other hand, S1P analogs with a short lipidic tail, such as d16:1 S1P and FTY720-P, induce $G_{12/13}$- and $G_{i/o}$-biased signaling via S1PR3.

17–induced ectodomain shedding of alkaline phosphatase–fused TGFα (AP-TGFα). As expected, both FTY720-P and d16:1 S1P lowered the maximal response of $G_{q/11}$ signaling by ~40% relative to d18:1 S1P. However, all compounds showed approximately equal maximal response via $G_{12/13}$ and $G_{i/o}$ signaling (Fig. 3B; fig. S4, B to D; and table S3). These data demonstrated that FTY720-P and d16:1 S1P are $G_{i/o}$- and $G_{12/13}$-biased agonists for S1PR3 (Fig. 3C). A previously determined sphingolipid-mimic antagonist–bound S1PR1 structure and docking simulations revealed that increased pocket-volume requirements for agonists drive the transition from an inactive to active conformation (*22*). Combined with the results in the present study, these findings suggest that biased signaling by shorter ligands is driven by lower pocket-volume requirements relative to d18:1 S1P.

Numerous S1P receptor modulators have been developed using the sphingosine backbone (*29*, *30*). One of these analogs (VPC23019) has a chemical structure similar to that of FTY720-P, except for the position of the alkyl tail (VPC23019 has it in the meta-position of the phenyl ring, whereas FTY720-P has it in the para-position) (Fig. 3A). Here, VPC23019 exhibited a lower potency in $G_{12/13}$ and $G_{i/o}$ signaling and no ability to initiate $G_{q/11}$ signaling as compared to FTY720-P, suggesting that both length and chemical structure of hydrophobic tail moiety affect ligand activity (fig. S4, B to D, and table S3).

S1PR-activation mechanism

Comparison of the agonist d18:1 S1P in S1PR3 with the antagonist ML056 in S1PR1 indicated that the alkyl tail of ligands strongly affects receptor activation (Fig. 4). The alkyl tail of d18:1 S1P exhibits an unbent conformation in active S1PR3 and is inserted into the gap between TM4 and TM5. In contrast, ML056 exhibits a bent conformation accommodated in the short hydrophobic pocket in S1PR1 (Fig. 4A). To accommodate d18:1 S1P in this conformation, four residues in S1PR3 (Leu122$^{3.36}$, Trp256$^{6.48}$, Phe204$^{5.47}$, and Phe260$^{6.52}$) are positioned differently from their positions in the inactive S1PR1. The side chains of Leu122$^{3.36}$ and Phe204$^{5.47}$ rotate toward TM1 and TM6, respectively, because of steric hindrance with the alkyl tail of d18:1 S1P. Simultaneously, Trp256$^{6.48}$ swings away

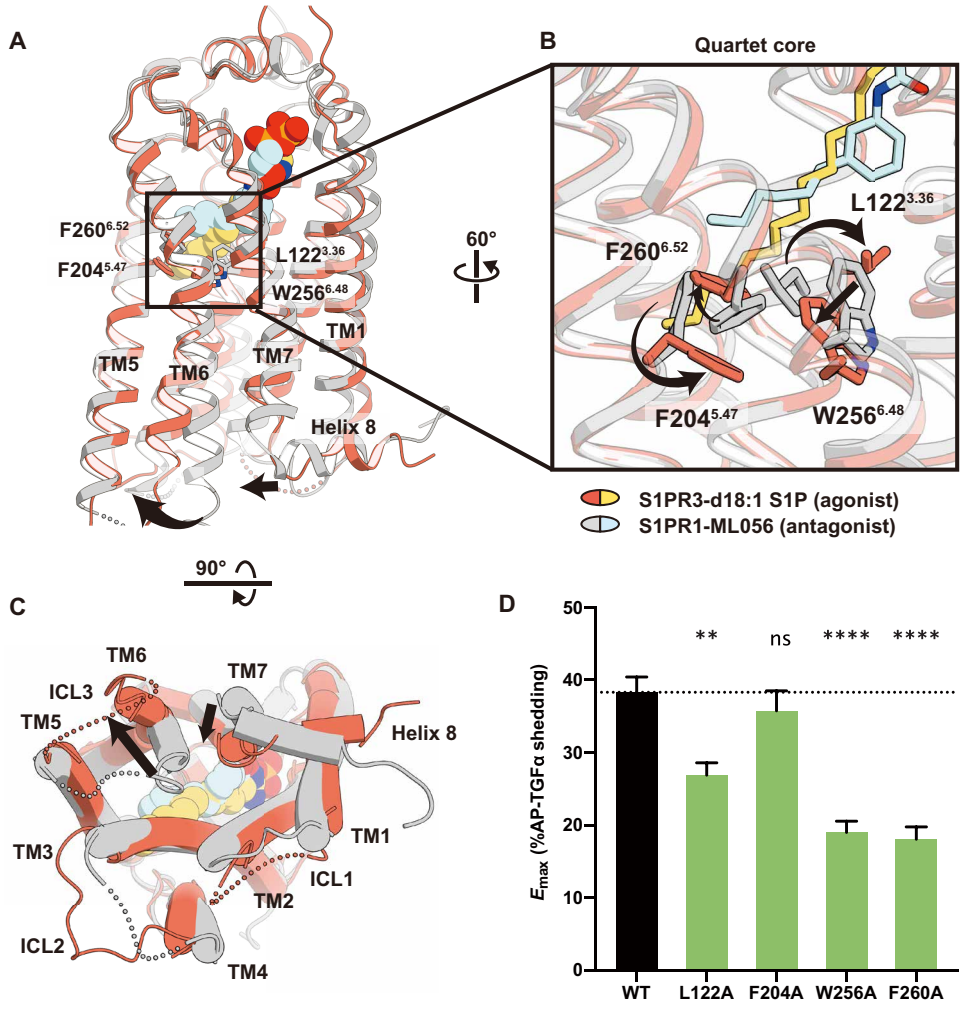

Fig. 4. S1PR-activation mechanism. (**A**) Superposition of the S1PR3 (dark salmon) and S1PR1 (3V2Y, dark gray) structures. Each molecule is colored as follows: S1PR3, dark salmon; S1PR1, light gray; d18:1 S1P, yellow; and ML056, light blue. (**B**) Comparison of residues comprising the quartet core in active S1PR3 and inactive S1PR1 structures. Extracellular view of S1PR3 superposed on S1PR1. ECL, extracellular loop. (**C**) Intracellular view of S1PR3 superposed on S1PR1. ICL, intracellular loop. (**D**) Comparison of maximal response (E_{max}) of d18:1 S1P in TGFα shedding assay with HEK293 parental cells expressing mutant and wild-type S1PR3. $^{**}P < 0.01$, $^{****}P < 0.0001$, mutant versus wild-type (WT) E_{max} values according to one-way ANOVA and Dunnett's post test. n.s., not significant.

owing to steric hindrance with the flipped side chain of Leu122$^{3.36}$ (Fig. 4B). Although a similar structural rearrangement is observed in cannabinoid receptor 1 (CNR1) (*11*, *23*), Phe200$^{3.36}$ in CNR1 (Leu122$^{3.36}$ in S1PR3) is reportedly flipped by hydrophobic interaction with the dimethyl group of the agonist (fig. S5). The side chain of Phe204$^{5.47}$ is stabilized by a π-π interaction with Phe260$^{6.52}$ in the active S1PR3 structure, whereas in the inactive S1PR1 structure, Phe$^{5.47}$ plugs the gap between TM4 and TM5 (Fig. 4B). The Phe204$^{5.47}$-Phe260$^{6.52}$ interaction in S1PR3 opens the long and wide gap between TM4 and TM5 connecting to the membrane, which allows for the accommodation of S1P analogs with various alkyl tail lengths (*31*) (fig. S6, A and B).

During the conformational change of the four residues upon the activation of receptor, TM6 is displaced outward by ~11 Å, and a partially unwound TM7 shifts inward by ~2.8 Å (Fig. 4C). Rearrangements of conserved activation motifs (P-I-F, sodium-binding site, D/E-R-Y, and NPxxY) within class A GPCRs are also similar to previously reported active GPCR structures (fig. S6, C to G) (*32*–*34*). Consistent with this model, alanine substitution of these four residues, except for Phe204$^{5.47}$, reduced maximal response to d18:1 S1P relative to that on wild-type S1PR3 (Fig. 4D). As these four residues concertedly alter their side-chain position to form an active conformation for G protein coupling, we referred to them as the "quartet core."

The role of the quartet core for G protein selectivity

The quartet core is located in proximity to the alkyl tail of d18:1 S1P, suggesting a possible role in lipid length–dependent G protein–subtype bias. To reveal the residues involved in determining $G_{i/o}$- and $G_{12/13}$-biased signaling, we performed a TGFα shedding assay using $G_{q/11}$- and $G_{12/13}$-deficient cells ($\Delta G_{q/11}$ and $\Delta G_{12/13}$). Among the four residues of the quartet core, alanine substitution of Leu122$^{3.36}$ decreased only $G_{q/11}$-signaling efficacy and maintained equivalent $G_{12/13}$-signaling efficacy in response to d18:1 S1P as compared with wild-type S1PR3 (Fig. 5, A to C, and table S4). This effect is similar to that caused by short lipidic agonists (FTY720-P and d16:1 S1P),

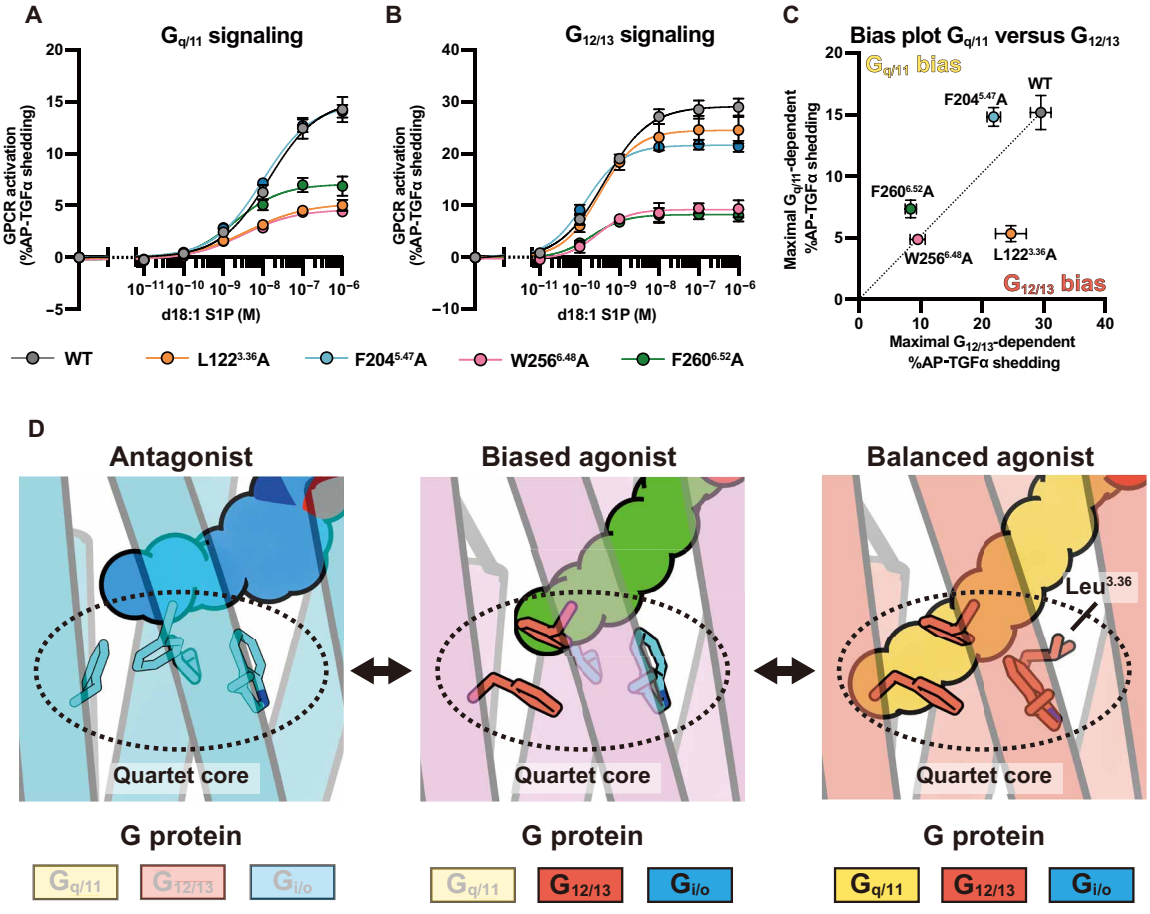

Fig. 5. The quartet core and biased agonism. (**A**) WT and mutant S1PR3 were examined for d18:1 S1P–induced AP-TGFα shedding responses in the $G_{12/13}$-knockout HEK293 cell line, reflecting $G_{q/11}$-mediated signaling. (**B**) WT and mutant S1PR3 were examined for d18:1 S1P–induced AP-TGFα shedding responses in the $G_{q/11}$-knockout HEK293 cell line, reflecting $G_{12/13}$-mediated signaling. Symbols and error bars in (A) and (B) represent mean and SEM, respectively, of three to six independent experiments with each performed in triplicate. Each line represents WT and mutant S1PR3 and is colored as follows: WT, gray; Leu122Ala, orange; Phe204Ala, light blue; Trp256Ala, pink; and Phe260Ala, green. (**C**) Bias plot of mutant and WT S1PR3 of maximal $G_{q/11}$-dependent % AP-TGFα shedding versus maximal $G_{12/13}$-dependent % AP-TGFα shedding. Symbols and error bars represent mean of maximal response and SEM in TGFα shedding assay with HEK293 $\Delta G_{12/13}$ or $\Delta G_{q/11}$ cell lines. Leu122Ala mutant shows $G_{12/13}$-biased activity. Phe204Ala mutant shows similar response to WT in both assays. Phe260Ala and Trp256Ala mutants show lower activity in both assays than WT. (**D**) Schematic models of S1PR3 activation and G protein–subtype bias. S1PR3 cannot couple to any G proteins in the antagonist-bound state (left). S1PR3 couples only to $G_{12/13}$ and $G_{i/o}$ upon binding to an agonist with a shorter lipidic chain, such as d16:1 S1P or FTY720-P (middle). S1PR3 couples with $G_{q/11}$, $G_{i/o}$, and $G_{12/13}$ upon binding to the major natural ligand 18:1 S1P (right).

suggesting that the interaction between Leu122$^{3.36}$ and agonists is important for $G_{q/11}$ signaling in S1PR3 (Fig. 3, A to C). In contrast, alanine substitution of both Trp256$^{6.48}$ and Phe260$^{6.52}$ decreased both $G_{q/11}$- and $G_{12/13}$-signaling efficacy in response to d18:1 S1P, whereas alanine substitution of Phe204$^{5.47}$ showed little effect on both $G_{q/11}$- and $G_{12/13}$-signaling efficacy (Fig. 5, A to C). These data suggest that Trp256$^{6.48}$ and Phe260$^{6.52}$ are responsible for S1PR3 forming an active conformation capable of coupling with all $G_{q/11}$, $G_{i/o}$, and $G_{12/13}$ subfamilies and that Leu122$^{3.36}$ specifically plays an important role in $G_{q/11}$ signaling (Fig. 5, A to C).

DISCUSSION

Recent advances in lipidomics analysis revealed that S1P analogs (d16:1, d17:1, d18:0, d18:2, and d20:1 in addition to d18:1 S1P) are present in mammalian blood plasma (*35*). Among these, the level of d16:1 S1P, which is normally present in very small amounts in physiological conditions, is reportedly increased under platinum-based chemotherapy and is associated with chemotherapy-induced peripheral neuropathy (*36*). The results of the present study revealed d16:1 S1P as a $G_{i/o}$- and $G_{12/13}$-biased agonist for S1PR3, whereas S1P analogs, which have a lipid tail with 18 or more carbons such as d18:0 S1P and d20:1 S1P, are balanced agonists (Fig. 3 and fig. S7). These findings suggest that modifying signaling bias offers a potential therapeutic strategy. Biased agonism in S1PRs is affected by various factors, including chaperone-dependent stability of S1P (*37*, *38*). Although our findings described structural mechanism of ligand-dependent biased agonism in S1PR3, the mechanism of chaperone-related biased agonism is still unclear. Further research is required to enhance our understanding of biased agonism of S1PRs in a biological system.

Among ~800 GPCRs, at least 36 recognize lipids (*39*, *40*). Although these lipid GPCRs regulate important physiological and pharmacological functions, there is little information available on their

structure as compared with those for amine and peptide GPCRs (*41*). Previous studies provided structural insights into the activation mechanism of some lipid GPCRs. The agonist-bound structure of prostaglandin E receptor 3 (PTGER3) suggests that direct interaction between the agonist and Trp$^{6.48}$ is important for activation (*24*, *25*, *42*). Moreover, in cannabinoid receptors, Phe$^{3.36}$-Trp$^{6.48}$ interaction plays a pivotal role in activation (*11*, *12*, *23*). In the present study, the d18:1 S1P–bound S1PR3 structure provided insight into a unique mechanism for lipid GPCR activation. In the active S1PR3 structure, d18:1 S1P dynamically rearranges four residues (termed the quartet core) in the lower part of the ligand-binding pocket, resulting in the formation of a long tunnel obliquely crossing S1PR3. Simultaneously, these rearrangements promote the active conformation, thereby explaining why S1PRs are activated by S1P analogs of varying lengths, even d20:1 S1P (*31*). There is, however, a caveat that the agonist-induced receptor activation mechanism dependent on the quartet core is specific for S1PR3 since we just compared the active S1PR3 structure and the inactive S1PR1 structure. To assess whether this proposed mechanism is correct and shared with other lipid GPCRs, further structural works on inactive conformations of S1PR3 and active conformations of other lipid GPCRs are required.

We also revealed that Leu122$^{3.36}$ in S1PR3 plays an important role in $G_{q/11}$ signaling. Short lipidic agonists lose the ability to interact with Leu122$^{3.36}$, resulting in greater $G_{12/13}$- and $G_{i/o}$-mediated activation rather than $G_{q/11}$. Angiotensin II (AngII) receptors (AGTR1 and AGTR2) show a similar mechanism for weaker $G_{q/11}$ signaling (*43*–*45*). In the antagonist-bound structure, Leu112$^{3.36}$ in AGTR1 (Leu122 in S1PR3) is near TM4, whereas the balanced agonist AngII changes the side-chain orientation of Leu112$^{3.36}$ from being near TM4 to TM7 (fig. S8A). However, the biased agonist TRV026 induces a distinct active conformation, including orientation of the Leu112$^{3.36}$ side chain in the proximal TM4 region, similar to that observed in the antagonist-bound structure (fig. S8A). These observations suggest that, in S1PR3, Leu122$^{3.36}$ is similarly involved in biased signaling (Fig. 5D). In many $G_{q/11}$-coupling class A GPCRs, the residue corresponding to Leu122$^{3.36}$ in S1PR3 is a conserved short aliphatic residue, such as Leu, Met, or Val, suggesting that $G_{q/11}$-coupling GPCRs share a similar mechanism underlying ligand-dependent biased signaling (fig. S8B). The findings in the present study can potentially promote the design of G protein subtype–biased agonists for optimized therapeutics targeting GPCRs.

MATERIALS AND METHODS

Expression construct amino acid sequence

The sequence cloned into pFastBac1 vector (Thermo Fisher Scientific) encoded *Homo sapiens* S1PR3 residues 2 to 315 of the total 378 residues (UniProt accession: Q99500), which are underlined in the sequence provided below. Hemagglutinin (HA) signal sequences and the FLAG epitope sequence on the N terminus, and enhanced green fluorescent protein sequence and 8 × poly-histidine tag on the C terminus of the receptor were retained after the tobacco etch virus (TEV) cleavage site. For removal of glycosylation, the Asn15Gln mutation was induced, which is in italics in the sequence provided below. Details of the cloning procedure are included in the following section.

KTIIALSYIFCLVFADYKDDDDKENLYFQGTSATALPPRLQPVRG*Q*ETLREHYQYVGKLAGRLKEASEGSTLTTVLFLVICSFIVLENLMVLIAIWKNNKFHNRMYFFIGNLALCDLLAGIAYKVNILMSGKKTFSLSPTVWFLREGSMFVALGASTCSLLAIAIERHLTMIKMRPYDANKRHRVFLLIGMCWLIAFTLGALPILGWNCLHNLPDCSTILPLYSKKYIAFCISIFTAILVTIVILYARIYFLVKSSSRKVANHNNSERSMALLRTVVIVVSVFIACWSPLFILFLIDVACRVQACPILFKAQWFIVLAVLNSAMNPVIYTLASKEMRRAFFRLVCNLEENLYFQGQFSKGEELFTGVVPILVELDGDVNGHKFSVSGEGEGDATYGKLTLKFICTTGKLPVPWPTLVTTFGYGVQCFARYPDHMKQHDFFKSAMPEGYVQERTIFFKDDGNYKTRAEVKFEGDTLVNRIELKGIDFKEDGNILGHKLEYNYNSHNVYIMADKQKNGIKVNFKIRHNIEDGSVQLADHYQQNTPIGDGPVLLPDNHYLSTQSALSKDPNEKRDHMVLLEFVTAAGITHGMDELYKHHHHHHHH-

Fab light chain

The sequence of the Fab AS55 fragment light chain is provided below. The complementarity-determining regions (CDRs) CDR-L1, CDR-L2, and CDR-L3 are underlined. The residues interacting with S1PR3 are shown in bold (fig. S2).

DIVMTQSPKSMSMSVGERVTLSCKASENVGIFVSWYQQKPEQSPKLLIYGASNRYTGVPDRFTGSGSATDFTLTLSSVQAEDLADYYCGQS**YNY**PLTFGAGTKLELKRADAAPTVSIFPPSSEQLTSGGASVVCFLNNFYPKDINVKWKIDGSERQNGVLNSWTDQDSKDSTYSMSSTLTLTKDEYERHNSYTCEATHKTSTSPIVKSFNRNEC

Fab heavy chain

The sequence of the Fab AS55 fragment heavy chain is provided below. CDR-H1, CDR-H2, and CDR-H3 are underlined. The residues interacting with S1PR3 are shown in bold (fig. S2).

DVQLQQSGAELVRPGASVKLSCKASGYTF**TDYE**MHWVKQTPVHGLEWIGAI**DPE**TGGTAYSQKFKGKATKTADKSSSTAYMELRSLTSEDSAVYYCTIP**YYSNLR**FAYWGQGTLVTVSSAKTTPPSVYPLAPGCGDTTGSSVTLGCLVKGYFPESVTVTWNSGSLSSSVHTFPALLQSGLYTMSSSVTVPSSTWPSQTVTCSVAHPASSTTVDKKLEPS

S1PR3 expression and purification

P2 high-titer recombinant baculovirus (>10^8 viral particles/ml) was obtained following transposition and transfection. For the expression of recombinant S1PR3, *Spodoptera frugiperda* insect cells at 2×10^6 to 3×10^6 cells/ml were infected with high-titer viral stock at a multiplicity of infection of 1. Cells were harvested by centrifugation (7000*g* for 10 min at 4°C) and washed with phosphate-buffered saline (PBS) (8000*g* for 10 min at 4°C) at 72 hours after infection and stored at −80°C until use.

Harvested cells were resuspended with hypotonic buffer [10 mM Hepes (pH 7.5), 20 mM KCl, 10 mM $MgCl_2$, and protease inhibitor cocktail (PIC; no. 25955-11, Nacalai Tesque, Kyoto, Japan)] followed by homogenization and centrifugation (215,000*g* for 30 min at 4°C). Pellets were collected and washed twice to prepare membranes using high osmotic buffer [5 mM Hepes (pH 7.5), 0.5 M NaCl, 10 mM KCl, 5 mM $MgCl_2$, and PIC]. The washed membranes were resuspended in resuspension buffer [50 mM Hepes (pH 7.5) and 500 mM NaCl] supplemented with iodoacetamide (2 mg/ml) (no. 095-02891, Fujifilm Wako Pure Chemical Industries, Osaka, Japan). The membrane suspension was rotated for more than 12 hours at 4°C. The following day, an equivalent volume of solubilization buffer [50 mM Hepes

(pH 7.5), 500 mM NaCl, 2.0% *N*-dodecyl-β-D-maltoside (DDM; no. D310, Anatrace, Maumee, Ohio, USA), and 0.4% cholesterol hydrogen succinate (CHS)] was added and rotated for 2 hours at 4°C. Solubilized membranes were centrifuged (215,000*g* for 30 min at 4°C), and supernatants were incubated with TALON metal affinity resin (no. 635503, TaKaRa Bio, Shiga, Japan) that had been pre-equilibrated with the wash buffer [50 mM Hepes (pH 7.5), 500 mM NaCl, 0.1% DDM, 0.02% CHS, and 15 mM imidazole] for 2 hours at 4°C. The resin was washed twice with 5 column volumes of wash buffer, followed by 2.5 column volumes of elution buffer (25 mM Hepes, 400 mM NaCl, 0.03% DDM, 0.006% CHS, and 250 mM imidazole). The collected eluates were pooled and concentrated to 15 ml with a concentrator (Amicon Ultra-15 50 K, Merck Millipore, Darmstadt, Germany), and imidazole was removed using a HiPrep 26/10 Desalting column (GE Healthcare). The solution was digested with 10 μM d18:1 S1P (Cayman Chemical) and a twofold molar excess of TEV protease (12 to 16 hours, 4°C). The following day, the protein solution was applied to Ni-Sepharose 6 Fast Flow resin (GE Healthcare). Flow-through fractions were collected and concentrated to 5 ml with a concentrator (50 K) and further purified by SEC with HiLoad 16/600 Superdex 200 pg (GE Healthcare) in gel filtration buffer [25 mM Hepes (pH 7.5), 200 mM NaCl, and 0.03% DDM]. The peak fractions were collected and concentrated to 10 mg/ml for following experiments.

Preparation of monoclonal antibody AS55

All animal experiments described in this study conformed to the guidelines outlined in the Guide for the Care and Use of Laboratory Animals of Japan and were approved by the Kyoto University Animal Experimentation Committee (approval no. Medkyo18068).

S1PR3 (2-330) was used to prepare the monoclonal anti-S1PR3 antibody (AS series). Construct design, expression, and purification were performed according to the protocol described above. Purified S1PR3 was reconstructed in liposomes with a ratio of 20:1 egg phosphatidylcholine (Sigma-Aldrich) to monophosphoryl lipid A (Sigma-Aldrich). MRL/lpr mice were immunized with liposomal S1PR3. Spleen cells were collected from the immunized mice and fused with NS-1 myeloma cells. Hybridoma cell–produced antibodies were screened using liposome enzyme-linked immunosorbent assay, followed by fluorescence SEC and flow cytometry analysis. Monoclonal hit clones were obtained by limiting dilution. Last, we isolated four clones of S1PR3-selective antibodies, including the crystallizing agent AS55. For the crystallization trial, a large number of monoclonal antibodies were prepared from the ascites of nude mice. Monoclonal antibodies were initially purified with protein G resin, eluted with glycine buffer, digested with papain, immobilized on *N*-hydroxysuccinimide–Sepharose, and incubated for 3 hours at 37°C. Then, the digested immunoglobulin G (IgG) samples were subjected to SEC (Hiload 16/600 Superdex 200 pg). The fraction of Fab fragments was incubated with protein A to remove either the Fc fragment or the residual IgG.

Liposome enzyme-linked immunosorbent assay

Purified S1PR3 (2-330) was reconstituted into liposomes containing biotinylated phosphoethanolamine (no. 860562, Avanti Polar Lipids Inc.) and immobilized onto streptavidin-coated plates (no. 436014, Thermo Fisher Scientific). The supernatant of hybridoma cells was added to the plates and mixed with a microplate mixed at 4°C for 1 hour. After washing with PBS containing 1% bovine serum albumin (PBS-B) three times, horseradish peroxidase–conjugated goat anti-mouse IgG, Fcγ fragment–specific antibody (no. 115-035-071, Jackson Immune Research, West Grove, PA, USA) was added and mixed with a microplate mixer at 4°C for 1 hour. After washing with PBS-B three times, KPL SureBlue TMB (3,3′,5,5′-tetramethylbenzidine) microwell peroxidase substrate was added. After incubation at room temperature, the reaction was stopped with 2 M H_2SO_4. Each well was evaluated by reading the absorbance at 450 nm. To eliminate antibodies recognizing flexible loops, N and C termini, or unstructured regions of S1PR3, we performed the same experiments using S1PR3 (2-330) denatured with 1% sodium dodecyl sulfate.

Fluorescence SEC

Purified S1PR3 (2-330) was incubated with culture supernatant of hybridoma and fluorescein isothiocyanate (FITC)–conjugated AffiniPure Fab goat anti-mouse IgG (no. 115-097-003, Jackson Immune Research). Reaction mixture was analyzed with ENrich SEC 650 10 × 300 column (no. 7801650, Bio-Rad). Green fluorescence was detected during running time.

Flow cytometry analysis

Purified S1PR3 (2-330) was incubated with culture supernatant of hybridoma and FITC-conjugated AffiniPure Fab goat anti-mouse IgG (no. 115-097-003, Jackson Immune Research). The reaction mixture was analyzed with an ENrich SEC 650 10 × 300 column (no. 7801650, Bio-Rad). Green fluorescence was detected during the running time.

Crystallization

The protein complex was prepared by incubating S1PR3 with Fab AS55 at a molar ratio of 1:2 for 1.5 hours at 4°C. The protein solution was subjected to SEC (Superdex 200 Increase 10/300 GL, GE Healthcare). Two peak fractions containing the S1PR3–Fab AS55 complex and monomeric Fab AS55 were obtained and mixed again; the final ratio of S1PR3 to Fab AS55 was 1:3. This step was required for better crystal quality for sufficient diffraction. The mixed complex was concentrated to 20 mg/ml by ultrafiltration (Amicon Ultra-0.5 50 K, Millipore), and d18:1 S1P was added to a final concentration of 400 μM. Complex and host lipids (monoolein and cholesterol) were mixed at a protein-to-lipid ratio of 2:3 using a mixer that consisted of two 100-μl gas-tight syringes (Hamilton Company). The syringe containing the reconstituted LCP was loaded onto an automated crystallization robot (NT-8-LCP, Formulatrix), and 50 nl was dispensed onto 96-well glass sandwich crystallization plates (LD11-50, Molecular Dimensions), which were subsequently overlaid with 800 nl of reservoir solution. Diffraction-quality crystals of S1PR3–Fab AS55 were obtained under conditions of 36% polyethylene glycol (PEG) 400, 0.1 M tris-HCl (pH 8.0), and 80 mM lithium citrate tribasic. Crystals were collected within 3 weeks using mesh grid loops (MiTeGen) and flash-cooled in liquid nitrogen.

Structure determination

Diffraction data were collected at 100 K at the SPring-8 microfocus beamline BL32XU (Japan) (*46*), using an Eiger X 9M detector (DECTRIS). A microfocused beam with a size of 15 μm by 10 μm and a wavelength of 1 Å was used for both raster scan and data collection. A dataset with a total oscillation range of 10° and 0.1° oscillations per frame was collected from each crystal under the absorbed dose of 10 MGy. A total of 481 collected datasets with the automated

data collection system ZOO (*47*) were merged, integrated, and scaled using the KAMO system (*48*), which exploits BLEND (*49*), XDS, and XSCALE (*50*, *51*). The structure of the S1PR3–Fab AS55 complex was determined by molecular replacement with the program PHASER (*52*) using the atomic coordinates of Fab 4A03 [Protein Data Bank (PDB) ID 5XLI)] and S1PR1 (PDB ID 3V2Y) as the search model. The model was initially refined using the "jerry body" refinement function implemented in REFMAC5 (*53*). The reflection data with phase information from molecule replacement undergo the density modification and noncrystallographic symmetry averaging by DM and phenix.density_modification. The structure is rebuilt and refined by phenix.autobuild and Rosetta in the beginning. Simulated annealing is applied in the initial refinement to reduce model bias. Most of the following structure refinement is conducted by phenix.real_space_refine with calculated weighted $2F_{obs} - F_{calc}$ maps. The sharpened map is produced by phenix.auto_sharpen for guiding manual refinement in COOT. At the tail of the final refinement process, we use riding hydrogen for geometry regularization to reduce clash and outlier. Ligand d18:1 S1P has also been restricted with tight angle and torsion angle restrain to maintain reasonable geometry against relatively weak density map (see table S2). Refined structures were visualized with CueMol: Molecular Visualization Framework (http://cuemol.org/). The Cα root mean square deviation values of the degree of shifts of helices were calculated by UCSF Chimera (*54*). Cα was defined as follows: TM6 as 6.29 to 30 and 32 to 33 and TM7 as 7.49 to 7.53 in Ballesteros-Weinstein numbering (*26*).

TGFα shedding assay

For the S1PR3 receptor activity study, the gene encoding human S1PR3, which was codon-optimized to improve the expression level, was cloned into the pCAGGS expression vector. The signal sequence of influenza HA followed by a FLAG epitope tag was attached to the N terminus of S1PR3. Each point mutation was introduced into S1PR3 by site-directed mutagenesis by whole-plasmid polymerase chain reaction.

Human embryonic kidney (HEK) 293 cells were maintained in Dulbecco's modified Eagle's medium (DMEM, Nacalai Tesque) supplemented with 10% fetal bovine serum (FBS), penicillin (100 U/ml), and streptomycin (100 μg/ml) (Nacalai Tesque) in a 37°C incubator with 5% CO_2. Cells were passaged twice a week.

The TGFα shedding assay was performed as described previously (*27*). In brief, HEK293 $\Delta G_{q/11}$, $\Delta G_{12/13}$, $\Delta G_{q/11/12/13}$ (*28*), or parental cells were seeded in a six-well plate at a density of 3×10^5 cells per well (for parental and $\Delta G_{q/11}$) or 5×10^5 cells per well (for $\Delta G_{12/13}$ and $\Delta G_{q/11/12/13}$) and cultured for 24 hours at 37°C with 2 ml of low-glucose DMEM supplemented with 10% charcoal-stripped FBS [(CS-FBS), Invitrogen], penicillin (100 U/ml), and streptomycin (100 μg/ml) (Nacalai Tesque). The cells were transfected with a mixture of expression plasmid vectors encoding alkaline phosphatase (AP)–TGFα (625 ng per well in six-well plates hereafter, unless otherwise noted) and S1PR3 (250 ng per well), using 2.5 μl of Lipofectamine 3000 reagent, 1.75 μl of P3000 reagent (Thermo Fisher Scientific), and 250 μl of Opti-MEM I reduced serum medium (Thermo Fisher Scientific) according to the manufacturer's instructions. For the negative control, the AP-TGFα plasmid and the empty pCAGGS plasmid vector were transfected. After 24 hours of incubation, the cells were dissociated by TrypLE Express Enzyme (Thermo Fisher Scientific), neutralized with 10% CS-FBS containing DMEM, collected in a 15-ml tube, centrifuged, and resuspended in 8 ml of Hanks' balanced salt solution (HBSS, Nacalai Tesque) with Ca^{2+} and Mg^{2+} containing 5 mM Hepes at pH 7.4. After 10 min of incubation at room temperature to settle the spontaneous AP-TGFα release caused by trypsinization, the cells were centrifuged and resuspended in 10 ml of HBSS with Hepes. The cell suspension was seeded in a 96-well culture plate at a volume of 90 μl per well. After 30 min of preincubation in a CO_2 incubator, each ligand, diluted in HBSS with Hepes supplemented with 0.01% lipid-free bovine serum albumin (Wako), was added, and the plates were incubated at 37°C in the CO_2 incubator. The plates were centrifuged at 190*g* for 2 min, and 80 μl of supernatant was transferred to an empty 96-well conditioned media (CM) plate. The alkaline phosphatase reaction solution [10 mM *p*-nitrophenyl phosphate (*p*-NPP, Wako), 120 mM tris-HCl (pH 9.5), 40 mM NaCl, and 10 mM $MgCl_2$] was dispensed into the cell plates and the CM plates (80 μl per well). The absorbance at 405 nm (A_{405}) of the plates was measured using a microplate reader (ARVO X5, PerkinElmer), before and after a 1-hour incubation at room temperature. For each well measurement, the increase in the A_{405} over the 1-hour incubation with *p*-NPP (ΔA_{405}) was used to determine alkaline phosphatase activity, and the value from the CM plate was normalized by the total ΔA_{405}. AP-TGFα release was calculated by subtracting the spontaneous AP-TGFα accumulation under the vehicle-treated conditions from that in the compound-stimulated conditions.

GloSensor cAMP assay

The plasmid encoding human S1PR3 was the same as in TGFα shedding assay. pGloSensor 22F plasmid DNA and cAMP reagent were purchased from Promega.

HEK293 cells were maintained in DMEM (Nacalai Tesque) supplemented with 10% FBS, penicillin (100 U/ml), and streptomycin (100 μg/ml) (Nacalai Tesque) in a 37°C incubator with 5% CO_2. Cells were passaged twice a week.

HEK293 cells were seeded in a 100-mm tissue culture dish at a density of 1.5×10^6 cells per dish and cultured for 24 hours at 37°C with 10 ml of low-glucose DMEM supplemented with 10% CS-FBS (Invitrogen), penicillin (100 U/ml), and streptomycin (100 μg/ml) (Nacalai Tesque). The cells were transfected with a mixture of pGloSensor cAMP 22F plasmid (8 μg per dish) and expression plasmid vectors encoding S1PR3 (2 μg per dish) using 30 μl of Fugene HD transfection kit (Promega) and 650 μl of Opti-MEM I reduced serum medium (Thermo Fisher Scientific) according to the manufacturer's instructions. The negative control, the pGloSensor cAMP 22F plasmid, and the empty pCAGGS plasmid vector were transfected. After 24 hours of incubation, the cells were dissociated by TrypLE Express Enzyme (Thermo Fisher Scientific), neutralized with 1% CS-FBS containing CO_2-independent medium (Invitrogen), collected in a 15-ml tube, centrifuged, and washed with 5 ml PBS (−). Then, cells were resuspended in 1% CS-FBS and 2% GloSensor cAMP reagent containing CO_2-independent medium at 5×10^5 cells/ml and rotated at room temperature for 2 hours. Cell suspension was seeded to LUMITRAC 96-well white plate (Greiner) at a volume of 80 μl per well; 10× agonist diluted in HBSS with Hepes supplemented with 0.01% lipid-free bovine serum albumin (Wako) was added, and the plates were incubated at room temperature for 10 min. Ten microliters of 100 μM forskolin diluted in HBSS with Hepes supplemented with 0.01% lipid-free bovine serum albumin (Wako) was added to each well (final, 10 μM), and plates were incubated for 30 min at room temperature. The luminescence of the plates was

measured using a microplate reader (ARVO X5, PerkinElmer). The count of each well was normalized to that of wells treated with forskolin alone as 100%.

Statistical analysis

Concentration-response curves expressed in the TGFα shedding assay were fit to a nonlinear regression (four-parameter) model in Prism (v.8.30, GraphPad Software Inc.). For functional analysis of wild-type and S1PR3 mutants, pEC_{50} and E_{max} values were calculated from nonlinear regression (four-parameter) analysis of mean data from independent experiments performed in triplicate. Error bars denote SEM.

SUPPLEMENTARY MATERIALS

Supplementary material for this article is available at http://advances.sciencemag.org/cgi/content/full/7/24/eabf5325/DC1

View/request a protocol for this paper from *Bio-protocol*.

REFERENCES AND NOTES

1. W. I. Weis, B. K. Kobilka, The molecular basis of G protein–coupled receptor activation. *Annu. Rev. Biochem.* **87**, 897–919 (2018).
2. S. R. Neves, P. T. Ram, R. Iyengar, G protein pathways. *Science* **296**, 1636–1639 (2002).
3. W. M. Oldham, H. E. Hamm, Heterotrimeric G protein activation by G-protein–coupled receptors. *Nat. Rev. Mol. Cell Biol.* **9**, 60–71 (2008).
4. V. Isberg, C. de Graaf, A. Bortolato, V. Cherezov, V. Katritch, F. H. Marshall, S. Mordalski, J. P. Pin, R. C. Stevens, G. Vriend, D. E. Gloriam, Generic GPCR residue numbers: Aligning topology maps while minding the gaps. *Trends Pharmacol. Sci.* **36**, 22–31 (2015).
5. J. D. Urban, W. P. Clarke, M. von Zastrow, D. E. Nichols, B. Kobilka, H. Weinstein, J. A. Javitch, B. L. Roth, A. Christopoulos, P. M. Sexton, K. J. Miller, M. Spedding, R. B. Mailman, Functional selectivity and classical concepts of quantitative pharmacology. *J. Pharmacol. Exp. Ther.* **320**, 1–13 (2007).
6. L. Tan, W. Yan, J. D. McCorvy, J. Cheng, Biased ligands of G protein–coupled receptors (GPCRs): Structure-functional selectivity relationships (SFSRs) and therapeutic potential. *J. Med. Chem.* **61**, 9841–9878 (2018).
7. D. Wootten, A. Christopoulos, M. Marti-Solano, M. M. Babu, P. M. Sexton, Mechanisms of signaling and biased agonism in G protein–coupled receptors. *Nat. Rev. Mol. Cell Biol.* **19**, 638–653 (2018).
8. E. Lorenzen, E. Ceraudo, Y. A. Berchiche, C. A. Rico, A. Fürstenberg, T. P. Sakmar, T. Huber, G protein subtype–specific signaling bias in a series of CCR5 chemokine analogs. *Sci. Signal.* **11**, eaao6152 (2018).
9. S. G. F. Rasmussen, B. T. DeVree, Y. Zou, A. C. Kruse, K. Y. Chung, T. S. Kobilka, F. S. Thian, P. S. Chae, E. Pardon, D. Calinski, J. M. Mathiesen, S. T. A. Shah, J. A. Lyons, M. Caffrey, S. H. Gellman, J. Steyaert, G. Skiniotis, W. I. Weis, R. K. Sunahara, B. K. Kobilka, Crystal structure of the β 2 adrenergic receptor-Gs protein complex. *Nature* **477**, 549–555 (2011).
10. A. Glukhova, C. J. Draper-Joyce, R. K. Sunahara, A. Christopoulos, D. Wootten, P. M. Sexton, Rules of engagement: GPCRs and G proteins. *ACS Pharmacol. Transl. Sci.* **1**, 73–83 (2018).
11. K. K. Kumar, M. Shalev-Benami, M. J. Robertson, H. Hu, S. D. Banister, S. A. Hollingsworth, N. R. Latorraca, H. E. Kato, D. Hilger, S. Maeda, W. I. Weis, D. L. Farrens, R. O. Dror, S. V. Malhotra, B. K. Kobilka, G. Skiniotis, Structure of a signaling cannabinoid receptor 1-G protein complex. *Cell* **176**, 448–458.e12 (2019).
12. C. Xing, Y. Zhuang, T.-H. Xu, Z. Feng, X. E. Zhou, M. Chen, L. Wang, X. Meng, Y. Xue, J. Wang, H. Liu, T. F. McGuire, G. Zhao, K. Melcher, C. Zhang, H. E. Xu, X.-Q. Xie, Cryo-EM structure of the human cannabinoid receptor CB2-Gi signaling complex. *Cell* **180**, 645–654.e13 (2020).
13. S. Maeda, Q. Qu, M. J. Robertson, G. Skiniotis, B. K. Kobilka, Structures of the M1 and M2 muscarinic acetylcholine receptor/G-protein complexes. *Science* **364**, 552–557 (2019).
14. W. J. Lennarz, Lipid metabolism. *Annu. Rev. Biochem.* **39**, 359–388 (1970).
15. H. Rosen, R. C. Stevens, M. Hanson, E. Roberts, M. B. A. Oldstone, Sphingosine-1-phosphate and its receptors: Structure, signaling, and influence. *Annu. Rev. Biochem.* **82**, 637–662 (2013).
16. V. A. Blaho, T. Hla, An update on the biology of sphingosine 1-phosphate receptors. *J. Lipid Res.* **55**, 1596–1608 (2014).
17. J. Chun, E. J. Goetzl, T. Hla, Y. Igarashi, K. R. Lynch, W. Moolenaar, S. Pyne, G. Tigyi, International Union of Pharmacology. XXXIV. Lysophospholipid receptor nomenclature. *Pharmacol. Rev.* **54**, 265–269 (2002).
18. C. Nussbaum, S. Bannenberg, P. Keul, M. H. Gräler, C. F. Gonçalves-de-Albuquerque, H. Korhonen, K. von Wnuck Lipinski, G. Heusch, H. C. de Castro Faria Neto, I. Rohwedder, J. R. Göthert, V. P. Prasad, G. Haufe, B. Lange-Sperandio, S. Offermanns, M. Sperandio, B. Levkau, Sphingosine-1-phosphate receptor 3 promotes leukocyte rolling by mobilizing endothelial P-selectin. *Nat. Commun.* **6**, 6416 (2015).
19. H. Okamoto, N. Takuwa, T. Yokomizo, N. Sugimoto, S. Sakurada, H. Shigematsu, Y. Takuwa, Inhibitory regulation of rac activation, membrane ruffling, and cell migration by the G protein-coupled sphingosine-1-phosphate receptor EDG5 but not EDG1 or EDG3. *Mol. Cell. Biol.* **20**, 9247–9261 (2000).
20. N. Sugimoto, N. Takuwa, H. Okamoto, S. Sakurada, Y. Takuwa, Inhibitory and stimulatory regulation of rac and cell motility by the G12/13-Rho and Gi pathways integrated downstream of a single G protein-coupled sphingosine-1-phosphate receptor isoform. *Mol. Cell. Biol.* **23**, 1534–1545 (2003).
21. S. C. Sensken, C. Stäubert, P. Keul, B. Levkau, T. Schöneberg, M. H. Gräler, Selective activation of G alpha i mediated signaling of S1P3 by FTY720-phosphate. *Cell. Signal.* **20**, 1125–1133 (2008).
22. M. A. Hanson, C. B. Roth, E. Jo, M. T. Griffith, F. L. Scott, G. Reinhart, H. Desale, B. Clemons, S. M. Cahalan, S. C. Schuerer, M. G. Sanna, G. W. Han, P. Kuhn, H. Rosen, R. C. Stevens, Crystal structure of a lipid G protein–coupled receptor. *Science* **335**, 851–855 (2012).
23. T. Hua, K. Vemuri, S. P. Nikas, R. B. Laprairie, Y. Wu, L. Qu, M. Pu, A. Korde, S. Jiang, J.-H. Ho, G. W. Han, K. Ding, X. Li, H. Liu, M. A. Hanson, S. Zhao, L. M. Bohn, A. Makriyannis, R. C. Stevens, Z.-J. Liu, Crystal structures of agonist-bound human cannabinoid receptor CB 1. *Nature* **547**, 468–471 (2017).
24. K. Morimoto, R. Suno, Y. Hotta, K. Yamashita, K. Hirata, M. Yamamoto, S. Narumiya, S. Iwata, T. Kobayashi, Crystal structure of the endogenous agonist-bound prostanoid receptor EP3. *Nat. Chem. Biol.* **15**, 8–10 (2019).
25. M. Audet, K. L. White, B. Breton, B. Zarzycka, G. W. Han, Y. Lu, C. Gati, A. Batyuk, P. Popov, J. Velasquez, D. Manahan, H. Hu, U. Weierstall, W. Liu, W. Shui, V. Katritch, V. Cherezov, M. A. Hanson, R. C. Stevens, Crystal structure of misoprostol bound to the labor inducer prostaglandin E 2 receptor. *Nat. Chem. Biol.* **15**, 11–17 (2019).
26. J. A. Ballesteros, H. Weinstein, in *Methods in Neurosciences*, S. C. B. T.-M. in N. Sealfon, Ed. (Academic Press, 1995), vol. 25, pp. 366–428.
27. A. Inoue, J. Ishiguro, H. Kitamura, N. Arima, M. Okutani, A. Shuto, S. Higashiyama, T. Ohwada, H. Arai, K. Makide, J. Aoki, TGFα shedding assay: An accurate and versatile method for detecting GPCR activation. *Nat. Methods* **9**, 1021–1029 (2012).
28. A. Inoue, F. Raimondi, F. M. N. Kadji, G. Singh, T. Kishi, A. Uwamizu, Y. Ono, Y. Shinjo, S. Ishida, N. Arang, K. Kawakami, J. S. Gutkind, J. Aoki, R. B. Russell, Illuminating G-protein coupling selectivity of GPCRs. *Cell* **177**, 1933–1947.e25 (2019).
29. M. D. Davis, J. J. Clemens, T. L. Macdonald, K. R. Lynch, Sphingosine 1-phosphate analogs as receptor antagonists. *J. Biol. Chem.* **280**, 9833–9841 (2005).
30. M. Jongsma, J. van Unen, P. van Loenen, M. C. Michel, S. L.-M. Peters, A. E. Alewijnse, Different response patterns of several ligands at the sphingosine-1-phosphate receptor subtype 3 (S1P3). *Br. J. Pharmacol.* **156**, 1305–1311 (2009).
31. A. Troupiotis-Tsaïlaki, J. Zachmann, I. González-Gil, A. Gonzalez, S. Ortega-Gutiérrez, M. L. López-Rodríguez, L. Pardo, C. Govaerts, Ligand chain length drives activation of lipid G protein-coupled receptors. *Sci. Rep.* **7**, 2020 (2017).
32. Q. Zhou, D. Yang, M. Wu, Y. Guo, W. Guo, L. Zhong, X. Cai, A. Dai, W. Jang, E. I. Shakhnovich, Z.-J. Liu, R. C. Stevens, N. A. Lambert, M. M. Babu, M.-W. Wang, S. Zhao, Common activation mechanism of class a GPCRs. *eLife* **8**, e50279 (2019).
33. B. Trzaskowski, D. Latek, S. Yuan, U. Ghoshdastider, A. Debinski, S. Filipek, Action of molecular switches in GPCRs—Theoretical and experimental studies. *Curr. Med. Chem.* **19**, 1090–1109 (2012).
34. S. Filipek, Molecular switches in GPCRs. *Curr. Opin. Struct. Biol.* **55**, 114–120 (2019).
35. P. Narayanaswamy, S. Shinde, R. Sulc, R. Kraut, G. Staples, C. H. Thiam, R. Grimm, B. Sellergren, F. Torta, M. R. Wenk, Lipidomic "deep profiling": An enhanced workflow to reveal new molecular species of signaling lipids. *Anal. Chem.* **86**, 3043–3047 (2014).
36. W. Wang, P. Xiang, W. S. Chew, F. Torta, A. Bandla, V. Lopez, W. L. Seow, B. W. S. Lam, J. K. Chang, P. Wong, K. Chayaburakul, W.-Y. Ong, M. R. Wenk, R. Sundar, D. R. Herr, Activation of sphingosine 1-phosphate receptor 2 attenuates chemotherapy-induced neuropathy. *J. Biol. Chem.* **295**, 1143–1152 (2020).
37. A. Cartier, T. Hla, Sphingosine 1-phosphate: Lipid signaling in pathology and therapy. *Science* **366**, eaar5551 (2019).
38. S. Galvani, M. Sanson, V. A. Blaho, S. L. Swendeman, H. Obinata, H. Conger, B. Dahlbäck, M. Kono, R. L. Proia, J. D. Smith, T. Hla, HDL-bound sphingosine 1-phosphate acts as a biased agonist for the endothelial cell receptor S1P1 to limit vascular inflammation. *Sci. Signal.* **8**, ra79 (2015).
39. S. P. H. Alexander, A. Christopoulos, A. P. Davenport, E. Kelly, N. V. Marrion, J. A. Peters, E. Faccenda, S. D. Harding, A. J. Pawson, J. L. Sharman, C. Southan, J. A. Davies; CGTP Collaborators, THE CONCISE GUIDE TO PHARMACOLOGY 2017/18: G protein-coupled receptors. *Br. J. Pharmacol.* **174**, S17–S129 (2017).

40. C. Munk, E. Mutt, V. Isberg, L. F. Nikolajsen, J. M. Bibbe, T. Flock, M. A. Hanson, R. C. Stevens, X. Deupi, D. E. Gloriam, An online resource for GPCR structure determination and analysis. *Nat. Methods* **16**, 151–162 (2019).
41. M. Audet, R. C. Stevens, Emerging structural biology of lipid G protein-coupled receptors. *Protein Sci.* **28**, 292–304 (2019).
42. Y. Toyoda, K. Morimoto, R. Suno, S. Horita, K. Yamashita, K. Hirata, Y. Sekiguchi, S. Yasuda, M. Shiroishi, T. Shimizu, Y. Urushibata, Y. Kajiwara, T. Inazumi, Y. Hotta, H. Asada, T. Nakane, Y. Shiimura, T. Nakagita, K. Tsuge, S. Yoshida, T. Kuribara, T. Hosoya, Y. Sugimoto, N. Nomura, M. Sato, T. Hirokawa, M. Kinoshita, T. Murata, K. Takayama, M. Yamamoto, S. Narumiya, S. Iwata, T. Kobayashi, Ligand binding to human prostaglandin E receptor EP 4 at the lipid-bilayer interface. *Nat. Chem. Biol.* **15**, 18–26 (2019).
43. H. Asada, S. Horita, K. Hirata, M. Shiroishi, Y. Shiimura, H. Iwanari, T. Hamakubo, T. Shimamura, N. Nomura, O. Kusano-Arai, T. Uemura, C. Suno, T. Kobayashi, S. Iwata, Crystal structure of the human angiotensin II type 2 receptor bound to an angiotensin II analog. *Nat. Struct. Mol. Biol.* **25**, 570–576 (2018).
44. C. M. Suomivuori, N. R. Latorraca, L. M. Wingler, S. Eismann, M. C. King, A. L. W. Kleinhenz, M. A. Skiba, D. P. Staus, A. C. Kruse, R. J. Lefkowitz, R. O. Dror, Molecular mechanism of biased signaling in a prototypical G protein-coupled receptor. *Science* **367**, 881–887 (2020).
45. L. M. Wingler, M. A. Skiba, C. McMahon, D. P. Staus, A. L. W. Kleinhenz, C. M. Suomivuori, N. R. Latorraca, R. O. Dror, R. J. Lefkowitz, A. C. Kruse, Angiotensin and biased analogs induce structurally distinct active conformations within a GPCR. *Science* **367**, 888–892 (2020).
46. K. Hirata, Y. Kawano, G. Ueno, K. Hashimoto, H. Murakami, K. Hasegawa, T. Hikima, T. Kumasaka, M. Yamamoto, Achievement of protein micro-crystallography at SPring-8 beamline BL32XU. *J. Phys. Conf. Ser.* **425**, 012002 (2013).
47. K. Hirata, K. Yamashita, G. Ueno, Y. Kawano, K. Hasegawa, T. Kumasaka, M. Yamamoto, ZOO: An automatic data-collection system for high-throughput structure analysis in protein microcrystallography. *Acta Crystallogr. Sect. D* **75**, 138–150 (2019).
48. K. Yamashita, K. Hirata, M. Yamamoto, KAMO: Towards automated data processing for microcrystals. *Acta Crystallogr. Sect. D Struct. Biol.* **74**, 441–449 (2018).
49. J. Foadi, P. Aller, Y. Alguel, A. Cameron, D. Axford, R. L. Owen, W. Armour, D. G. Waterman, S. Iwata, G. Evans, Clustering procedures for the optimal selection of data sets from multiple crystals in macromolecular crystallography. *Acta Crystallogr. Sect. D Biol. Crystallogr.* **69**, 1617–1632 (2013).
50. W. Kabsch, Automatic processing of rotation diffraction data from crystals of initially unknown symmetry and cell constants. *J. Appl. Crystallogr.* **26**, 795–800 (1993).
51. W. Kabsch, Integration, scaling, space-group assignment and post-refinement. *Acta Crystallogr. Sect. D Biol. Crystallogr.* **66**, 133–144 (2010).
52. A. J. McCoy, R. W. Grosse-Kunstleve, P. D. Adams, M. D. Winn, L. C. Storoni, R. J. Read, Phaser crystallographic software. *J. Appl. Crystallogr.* **40**, 658–674 (2007).
53. G. N. Murshudov, P. Skubák, A. A. Lebedev, N. S. Pannu, R. A. Steiner, R. A. Nicholls, M. D. Winn, F. Long, A. A. Vagin, REFMAC5 for the refinement of macromolecular crystal structures. *Acta Crystallogr. Sect. D Biol. Crystallogr.* **67**, 355–367 (2011).
54. E. F. Pettersen, T. D. Goddard, C. C. Huang, G. S. Couch, D. M. Greenblatt, E. C. Meng, T. E. Ferrin, UCSF Chimera—A visualization system for exploratory research and analysis. *J. Comput. Chem.* **25**, 1605–1612 (2004).

Acknowledgments: We thank assistant technical staff H. Hisano at Kyoto University for supporting all experiments, especially antibody development and S1PR3 purification. We also thank BL32XU beamline scientists Y. Kawano and N. Sakai for assisting with x-ray crystallographic data collection. DNA sequencing analysis was performed at the Medical Research Support Center, Graduate School of Medicine, Kyoto University. We thank S. Narumiya for supervising S.M. **Funding:** This work was supported by the Platform for Drug Discovery, Informatics, and Structural Life Science from the Ministry of Education, Culture, Sports, Science, and Technology, Japan and by JSPS KAKENHI [grant nos. 19J22636 (S.M.), 18H02394 (E.N.), 17K08264 (A.I.), 19H05776 (S.I.), 19H05777 (S.I.), and 15H05721 (M.H.)]. This study was also supported by the Platform Project for Supporting Drug Discovery and Life Science Research [Basis for Supporting Innovative Drug Discovery and Life Science Research (BINDS)] from AMED [grant nos. JP20am0101070 (S.I. and K.H.), JP20am0101079 (S.I.), JP20am0101092 (M.H.), PRIME JP19gm5910013 (A.I.), and LEAP JP19gm0010004 (A.I. and J.A.)]. **Author contributions:** S.M., M.T., S.I., and M.H. designed the project; S.M., Y.S., and H.A. generated the hybridoma cells expressing anti-S1PR3; S.M., Y.S., and H.A. performed antibody purification and evaluation; S.M. and Y.S. performed cloning and expression of the Fab fragments; S.M. purified and crystallized the S1P–S1PR3–Fab AS55 complex; S.M. constructed the S1PR3 mutants and performed the TGFα shedding assays and statistical analyses; K.H. collected and processed the synchrotron data; S.M., H.A., and K.H. determined the initial complex structure; S.M., F.L., and E.N. refined the complex structure; F.L. and E.N. finalized the complex structure; N.T. supervised the chemical compound structure determination; A.I. provided G protein-knockout cell lines and plasmid vectors related to the TGFα shedding assay; S.M., S.I., and M.H. compiled the figures for the manuscript; and S.M., S.I., and M.H. wrote the manuscript. All authors reviewed the results, commented on the manuscript, and agreed on publication. **Competing interests:** S.M., S.I., and M.H. are inventors on a Japanese patent application related to this work filed by Kyoto University (no. 6990, filed 16 November 2020, waiting for publication). The other authors declare that they have no competing interests. **Data and materials availability:** Atomic coordinates and structure factors for the x-ray structures have been deposited in the PDB with accession no. 7C4S for the structure of the d18:1 S1P–bound S1PR3–Fab AS55 complex. Raw diffraction data for this structure have been deposited in CXIDB with accession ID 184 (https://cxidb.org/id-184.html). All data needed to evaluate the conclusions in the paper are present in the paper and/or the Supplementary Materials. The G protein-KO HEK293 cells and AP-TGFα shedding assay constructs are available from A.I. under a material transfer agreement with Tohoku University.

Submitted 2 November 2020
Accepted 21 April 2021
Published 9 June 2021
10.1126/sciadv.abf5325

Citation: S. Maeda, Y. Shiimura, H. Asada, K. Hirata, F. Luo, E. Nango, N. Tanaka, M. Toyomoto, A. Inoue, J. Aoki, S. Iwata, M. Hagiwara, Endogenous agonist–bound S1PR3 structure reveals determinants of G protein–subtype bias. *Sci. Adv.* **7**, eabf5325 (2021).

Science Advances

Endogenous agonist–bound S1PR3 structure reveals determinants of G protein–subtype bias

Shintaro Maeda, Yuki Shiimura, Hidetsugu Asada, Kunio Hirata, Fangjia Luo, Eriko Nango, Nobuo Tanaka, Masayasu Toyomoto, Asuka Inoue, Junken Aoki, So Iwata and Masatoshi Hagiwara

Sci Adv **7** (24), eabf5325.
DOI: 10.1126/sciadv.abf5325